

# Transition Prediction for Hypersonic Inlet

Huiyong Zhao, Miaorong Yi

Corresponding author: gmreszhao@cardc.cn

Science and Technology on Scramjet Laboratory of Hypervelocity Aerodynamics Institute of  
CARD, Mianyang Sichuan 621000, China.

**Abstract:** The reliable numerical prediction of the laminar-to-turbulent transition is a challenging and important task for hypersonic inlet. The  $\gamma$ - $Re_{\theta t}$  transition model of Langtry and Menter is improved with compressibility corrections of  $Re_{\theta t}$  and the cross-flow transition model. The transition of two hypersonic inlets are simulated with the present transition model. One inlet is from the Shock Wave Laboratory (SWL) of RWTH Aachen University in Mach 7.7 shock tunnel, and the other inlet is the 20% scaled X-51A forebody in the Boeing/AFOSR Mach-6 Quiet tunnel. The computational results show good agreement with experimental data. The present new correlation of  $Re_{\theta t}$  efficiently delays the transition than Langtry's correlation and gets a better result. For SWL inlet, the transitional flow has the middle inlet performance between the laminar flow and the turbulent flow. For X-51A inlet, the noisy mode has higher mass flux but lower mass averaged Mach number and recovery coefficient of total pressure than quiet mode. The effect of  $Tu$  on the inlet performance is also investigated for X-51A inlet.

*Keywords:* boundary layer Transition, Computational Fluid Dynamics, Hypersonic Inlet.

## 1 Introduction

For a scramjet inlet at flight condition, the state of the boundary layer (laminar, transitional or turbulent) plays an important role on many aspects including the size and location of flow separation, the surface heat loads, and the inlet performance. It is difficult to duplicate the flight conditions for ground facilities including the quiet wind tunnel. As a result, an accurate transition prediction method is necessary for the assessment of inlet starting capability and the design of thermal protection system.

Moreover, in order to reduce the susceptibility to flow separations of inlet and allow extrapolation of ground test results to flight, the boundary layer approaching the hypersonic inlet should be turbulent. According to the two flight tests of X-43A flight vehicle in 2004<sup>[1]</sup>, the boundary layer on the top surface of inlet without forced-transition trip remained laminar flow. On the contrary, the boundary layer on the bottom surface with trip was turbulent ahead of the inlet during critical portions of the trajectory. However, could the transition be achieved on the bottom surface without trip for other hypersonic inlets? If so, the trip is unnecessary. If not, transition trip is necessary. On account of huge expense of flight testing and inadequate simulation capability of ground facilities, the answer depends heavily on a reliable transition prediction method for a hypersonic inlet.

Recently, some researchers successfully predict transition for hypersonic inlet with transition model based on turbulence model. Frauholz<sup>[2]</sup> coupled the  $\gamma$ - $Re_{\theta t}$  transition model<sup>[3]</sup> of Langtry and Menter to a Reynolds stress turbulence model (RSM). He computed three hypersonic inlets from the Shock Wave Laboratory (SWL) of RWTH Aachen University, DLR and Russia ITAM, respectively. In contrast to fully turbulent computations, the transition model resulted in a better agreement with the

available experimental data. However, Frauholz<sup>[2]</sup> did not studied the effect of boundary layer states (laminar, transitional and turbulent) or free stream noise on the transition of inlet. Borg<sup>[4]</sup> investigated the effect of free-stream noise on transition region through an experiment for a 20% scaled X-51A forebody in the Boeing/AFOSR Mach-6 Quiet tunnel in 2008. This experiment provides a good validation data for transition model. Xiao<sup>[5]</sup> simulated the natural transition of X-51A forebody of Borg's experiment with a transition model of Wang<sup>[5]</sup>. He got good laminar result for test in quiet wind tunnel and captured the right transition onset in noisy wind tunnel, but the transition ending position was noticeable earlier than experimental data in noisy wind tunnel. Yi<sup>[7]</sup> captured well the natural and forced transition of X-51A forebody of Borg's experiment with  $\gamma$ - $Re_{\theta t}$  transition model. The above researches focused on the simulation of transition region of forebody or inlet, but not the effect of transition and freestream turbulence intensity on the inlet performance, which were critical for the design of inlet and forced-transition trip.

The aim of the paper is to improve the transition prediction for hypersonic inlet flow in comparison with the experimental data. Meantime, we study the effect of boundary layer state (laminar, transitional and turbulent flow) and the free-stream disturbances on the inlet performance.

In section 2, we improve the Langtry and Menter's  $\gamma$ - $Re_{\theta t}$  transition model<sup>[3]</sup> with compressibility corrections of  $Re_{\theta t}$  and cross flow transition model. In section 3, the transition model is validated with a hypersonic inlet model from the Shock Wave Laboratory (SWL) of RWTH Aachen University<sup>[2]</sup>. In section 4, the 20% scaled X-51A forebody and inlet is computed with the comparison of Borg's experimental transition region<sup>[4]</sup>. The computational results shows a good agreement with experimental data. In section 5, the conclusion is drawn, and the future work is envisioned.

## 2 Numerical Method

All of the computations within this paper is performed using a inhouse parallel CFD software AHL3D (Airbreathing Hypersonic Laboratory Three-Dimensional). The Favre-averaged compressible viscous Navier-Stokes equations are discretized by finite volume method on multi-block structured grid. The time integration method is the Lower/Upper Symmetric Gauss-Seidel (LU-SGS)<sup>[8]</sup>. The inviscid flux is calculated by Improved Advection Upstream Splitting Method (AUSMPW+)<sup>[9]</sup> with the 3<sup>rd</sup> reconstruction of Monotone Upwind Scheme of Conservation Law (MUSCL)<sup>[10]</sup>. The viscous flux is calculated by Gauss theorem. The parallel computation is achieved by Message Passing Interface (MPI).

Based on Menter's two-equation eddy viscosity SST turbulence model<sup>[11]</sup>, the  $\gamma$ - $Re_{\theta t}$  transition model of Langtry and Menter<sup>[3]</sup> provides two additional transport equations to model the transitional process. The  $\gamma$  intermittency equation triggers the transition process and controls the production of turbulent kinetic energy in the boundary layer. The transport equation for the transition onset Reynolds number  $Re_{\theta t}$  is used to capture the non-local effect of the freestream turbulence intensity and pressure gradient at the boundary layer edge. For the three dimensional inlet, cross-flow instability maybe induces transition. The  $\gamma$ - $Re_{\theta t}$  transition model is extended to model the cross-flow transition according to Langtry's method<sup>[8]</sup>. Since the  $\gamma$ - $Re_{\theta t}$  transition model is initially developed for the transition prediction of low speed flows, two compressibility corrections<sup>[13][14]</sup> were introduced into the transition model for the transition prediction of high speed flow.

Here, we only summarize the main transport equations of transition model following the notation of Langtry<sup>[3][8]</sup>. The reader could get the detailed formulation of the transition mode from reference [3] and [8].

$$\frac{\partial(\rho\gamma)}{\partial t} + \frac{\partial(\rho U_j \gamma)}{\partial x_j} = P_\gamma - E_\gamma + \frac{\partial}{\partial x_j} \left[ \left( \mu + \frac{\mu_t}{\sigma_f} \right) \frac{\partial \gamma}{\partial x_j} \right] \quad (1)$$

$$\frac{\partial(\rho \tilde{\text{Re}}_{\theta t})}{\partial t} + \frac{\partial(\rho U_j \tilde{\text{Re}}_{\theta t})}{\partial x_j} = P_{\theta t} + D_{scf} + \frac{\partial}{\partial x_j} \left[ \sigma_{\theta t} (\mu + \mu_t) \frac{\partial \tilde{\text{Re}}_{\theta t}}{\partial x_j} \right] \quad (2)$$

where the  $P_\gamma$  and  $E_\gamma$  in the equation (1) are the production and destruction terms, respectively.

$$P_\gamma = F_{length} c_{a1} \rho S [\gamma F_{onset}]^{0.5} (1 - c_{e1} \gamma) \quad (3)$$

$$E_\gamma = c_{a2} \rho \Omega \gamma F_{turb} (c_{e2} \gamma - 1) \quad (4)$$

The  $P_{\theta t}$  in the equation (2) is the production term of  $\tilde{\text{Re}}_{\theta t}$  equation.

$$P_{\theta t} = c_{\theta t} \frac{\rho}{t} (\text{Re}_{\theta t} - \tilde{\text{Re}}_{\theta t}) (1.0 - F_{\theta t}) \quad (5)$$

In the equation (5),  $\text{Re}_{\theta t}$  is the transition momentum thickness Reynolds number in the free-stream. It is determined by the free stream turbulence intensity  $Tu$  and the pressure gradient parameter  $\lambda_\theta$  as equation (6). In order to consider the effect of compressibility on transition for high speed flow, Zhang<sup>[13]</sup> and Zheng<sup>[14]</sup> modify the equation (6) to equation (7) with a function  $G$  of local Mach number as equation (8) and (9), respectively.

$$\text{Re}_{\theta t} = E(T_u) F(\lambda_\theta) \quad (6)$$

$$\text{Re}_{\theta t} = E(T_u) F(\lambda_\theta) G(Ma) \quad (7)$$

$$G(Ma) = 0.00987 Ma^3 - 0.14407 Ma^2 + 0.75109 Ma + 1 \quad (8)$$

$$G(Ma) = 0.00108 Ma^4 - 0.01824 Ma^3 + 0.08576 Ma^2 + 0.20011 Ma + 0.77679 \quad (9)$$

The  $D_{scf}$  in the equation (2) is the contribution term by a cross-flow model from Langtry<sup>[8]</sup>.

$$D_{SCF} = c_{\theta t} \frac{\rho}{t} c_{crossflow} \min(\text{Re}_{SCF} - \tilde{\text{Re}}_{\theta t}, 0.0) F_{\theta t 2} \quad (10)$$

The treatment of boundary conditions are as the below:

At the far field boundary, supersonic inflow or outflow conditions are imposed. The turbulent kinetic energy  $k_\infty$  are determined by the free stream turbulence intensity  $Tu$ . If the turbulence intensity is unavailable from experiments, one can use trial and error procedure to determine it according to the transition region from experiment. The specific dissipation rate of the free stream  $\omega_\infty$  is determined with given the ratio of turbulent to laminar viscosity in the free stream. At solid wall, the no-slip isothermal wall are imposed.

For the transitional variables, the free stream values of  $\gamma=1$ , the  $\tilde{\text{Re}}_{\theta t}$  is determined as Langtry<sup>[3]</sup>. For the supersonic outflow, the  $\gamma$  and  $\tilde{\text{Re}}_{\theta t}$  are extrapolated from the interior flow field. At no-slip wall, the  $\gamma$  is set to zero, and the normal gradient of  $\tilde{\text{Re}}_{\theta t}$  is set to zero.

### 3 Validation of Transition Model

The validation case is a hypersonic inlet from the Shock Wave Laboratory (SWL) of RWTH as Frauholz<sup>[2]</sup> did. Figure 1 shows the geometry of the SWL inlet. The model has two exterior compression ramps and an interior section (i.e. isolator). The leading edge of the first ramp and cowl lip are sharp. The model is 100mm wide and has straight side walls on both sides. The experiment was conducted in the hypersonic shock tunnel TH2 in Aachen.

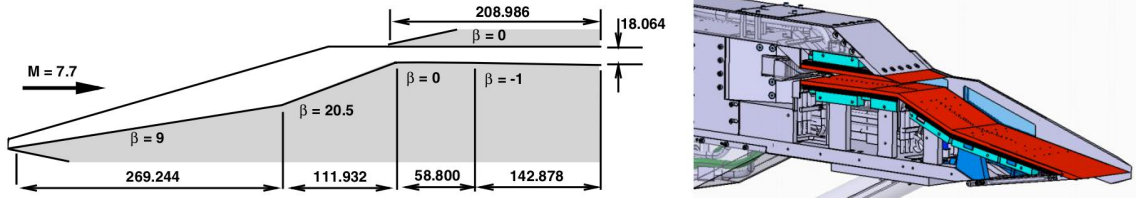


Figure 1: Geometry of the SWL inlet [2]

The inflow conditions are  $Ma=7.7$ ,  $Re_\infty=4.1 \cdot 10^6/m$  and  $T_i=1520K$ . The wall temperature is 300K.

The pressure and heat transfer rate are measured by Kulite pressure probes and thermocouples sensors along the center-line of the wall, respectively. Based on the measurement, the  $C_p$  and the Stanton number are calculated with the equation (11).

$$c_p = \frac{P - P_\infty}{0.5 \rho_\infty V_\infty^2} \quad St = \frac{q_w}{\rho_\infty |V_\infty| c_p (T_{t,\infty} - T_w)} \quad (11)$$

The total grid number is about 2.1 million. The grid number is 250 at the flow direction, 101 at the spanwise direction, and 61 at the normal direction. The  $y^+$  of the first layer of grid cells away from the wall are smaller than 1.

The overall flow phenomena can be seen in Figure 2-3. The flow field includes two oblique shock waves and two separation zone in black circles in Figure 3. The first shock wave is generated by the sharp leading edge. The second one is generated at the corner between two ramps. The first separation zone are at the corner between the first ramp and the second ramp. The second separation zone is at the entrance of the isolator.

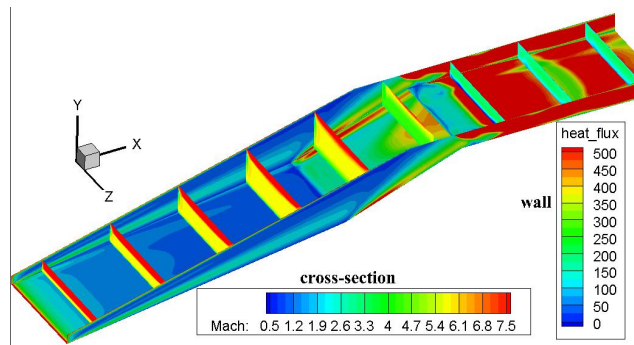


Figure 2: computed flow phenomenon of the SWL inlet (heat flux rate contour on the wall and Mach number contour on the cross-sections)

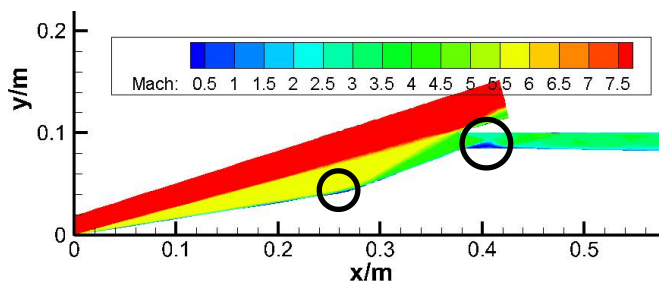


Figure 3: computed transitional Mach number contour at the symmetric plane of the SWL inlet

In order to analyze the transition region, the laminar, transitional and turbulent computation are conducted. In Figure 4, One side wall is hidden for better visualization. At the corner, the separation

zone is the largest for laminar flow, the smallest for turbulent flow, and the middle for transitional flow. At the isolator, Laminar flow has two large separation zone. One is at the entrance of the isolator because of the interaction between reflected oblique shock waves and the boundary layer, and the other is at the middle of isolator generated by the interaction between shock train and boundary layer. The flow are relatively simple for transitional and turbulent with a big separation zone and two corner separation zones near the side wall in the isolator entrance. The transition appears at the middle of the second ramp from the contour of heat transfer.

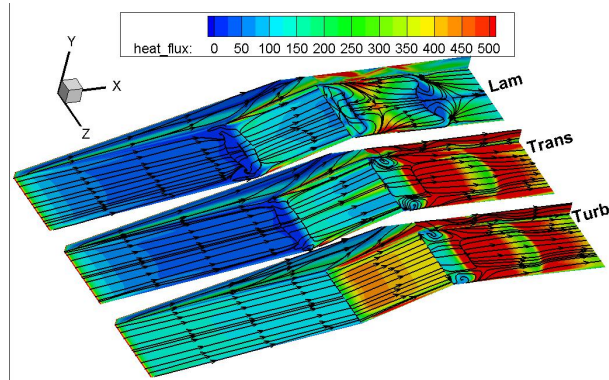


Figure 4: computed skin friction lines and heat transfer on the bottom wall plane of the SWL inlet

In Figure.5-6, the symbol “Test” denotes the experimental result of pressure coefficients. The line “Turb” and “Lam” denote the computed pressure coefficients for laminar and turbulent flow, respectively. The line “AHL3D” denotes the present computed transitional result. For comparison, line “QUADFLOW” denotes the computed transitional result of Frauholz[2].

From the left figure of Figure.5, the pressure remains constant at the first ramp. After the corner ( $x=0.269m$ ), the pressure increases by a small step on account of a oblique shock wave at the corner. At the entrance of the isolator, the pressure first decreases because of the flow separation then increase suddenly after the reflected shock wave from the cowl lip hits the bottom wall surface. Around the corner, the computed pressure coefficients seems to make no difference for different boundary layer state. However, after we zoom in the corner (from the right figure of Figure.5), the turbulent flow diminishes the separation zone around the corner, and the laminar flow has the largest separation zone. As Frauholz<sup>[2]</sup> pointed out that the transitional computation with QUADFLOW solver slightly overpredicted the size of the separation zone at the corner. The present computation correctly predicts the size of separation zone.

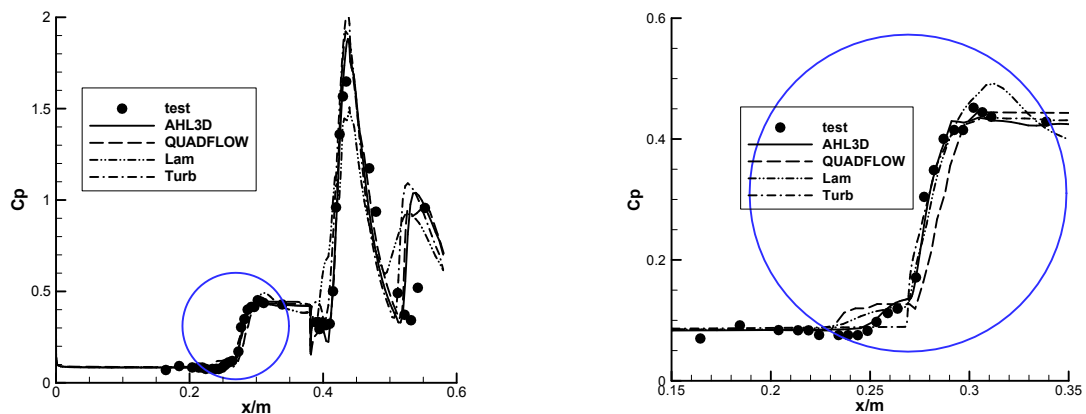


Figure 5: The pressure coefficients along the centerline of bottom wall plane of the SWL inlet (The left is the full graph, the right is the zoom-in at the corner between the first and the second ramp)

From the Figure. 6, the distribution of Stanton number seems like that of pressure coefficient

except the transition region. The transition starts at the corner, and finishes at the middle of the second ramp (about  $x=0.345\text{m}$ ). Because of a separation bubble at the corner, the transition could be induced by the separation. As Frauholz<sup>[2]</sup> pointed out that QUADFLOW solver predicted the correct transitional onset position but slight early transition finish position. The present computation correctly predicts the transition region. It should be noted that the present computation over-estimates the Stanton number at  $X=0.44\sim 0.46\text{m}$ . The reason is under the further investigation.

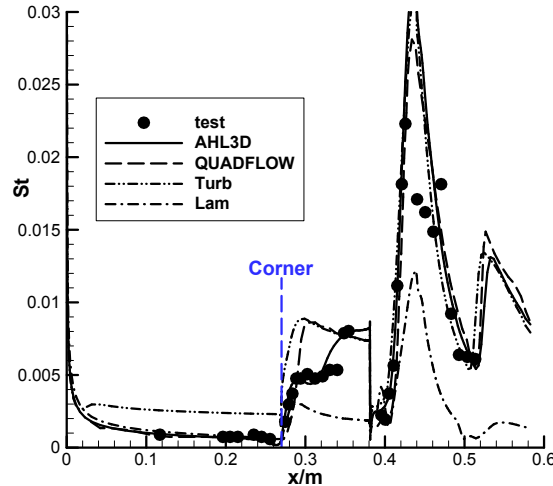


Figure 6: The Stanton number along the centerline of bottom wall plane of the SWL inlet

From Table. 1, the inlet performance is measured with the mass flux, mass averaged Mach number at the isolator exit (i.e.  $Mw Ma$ ) and the recovery coefficient of mass averaged total pressure at the isolator exit (i.e.  $\sigma$ ). The laminar flow has the highest mass flux,  $Mw Ma$  and  $\sigma$ , and the turbulent flow has the smallest mass flux,  $Mw Ma$  and  $\sigma$ . The transitional flow is between the laminar and turbulent flow and near the laminar flow.

Table 1 Effect of boundary layer state on inlet performance

Boundary Layer State	Mass flux/(kg/s)	$Mw Ma$	$\sigma$
Laminar	0.336	3.056	0.336
Transitional	0.336	2.980	0.336
Turbulent	0.325	2.772	0.325

## 4 Results and Discussion

### 4.1 20% scaled X-51A inlet Model and Experiment

Borg<sup>[4]</sup> studied the effect tunnel noise and the forced-transition trip on windward forebody transition for a 20% scaled X-51A inlet model (as shown in Figure.7) in Boeing/AFOSR Mach-6 Quiet tunnel. The wall temperature is measured with Temperature Sensitive Paint (TSP). The transition region is deduced from the distribution of wall temperature.



Figure 7: Photograph of windward side of the X-51A inlet model<sup>[4]</sup>

The inflow conditions under quiet mode are  $Ma=6$ ,  $P_t=586\text{kpa}$ ,  $T_t=418\text{K}$ ,  $Re=6.59 \cdot 10^6/\text{m}$  and noise level on the order of 0.05%, and those under noisy mode are  $Ma=5.8$ ,  $P_t=621\text{kpa}$ ,  $T_t=424\text{K}$ ,  $Re=7.4 \cdot 10^6/\text{m}$  and noise level on the order of 3%. The angle of attack is 4 degree for the test model.

In this section, the isolator is added to the computational model for research of inlet performance. Although the experiment includes the natural and forced transition, the only natural transitional

experimental results without trips are computed for simplicity in this paper.

From the Figure.8-9, the flow remains laminar at the forebody under quiet mode, whereas the flow transition starts at 134mm and finishes at 270mm away from the tip of model under noisy mode. Borg<sup>[4]</sup> believed that the compression corner ( $x=116\text{mm}$ ) almost certainly has a destabilizing effect on the boundary layer and the transition is induced by the corner. The large spikes on the Figure.9 are due to the registration marks on the model surface.

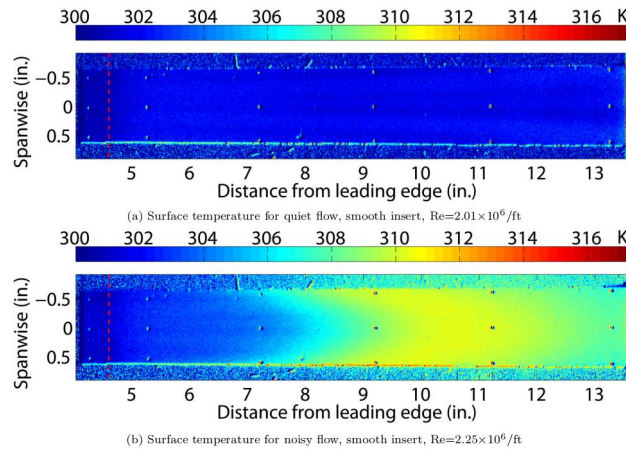


Figure 8: Surface temperature (K) under quiet (top) and noisy (bottom) conditions for the X-51A inlet (from Ref [4])

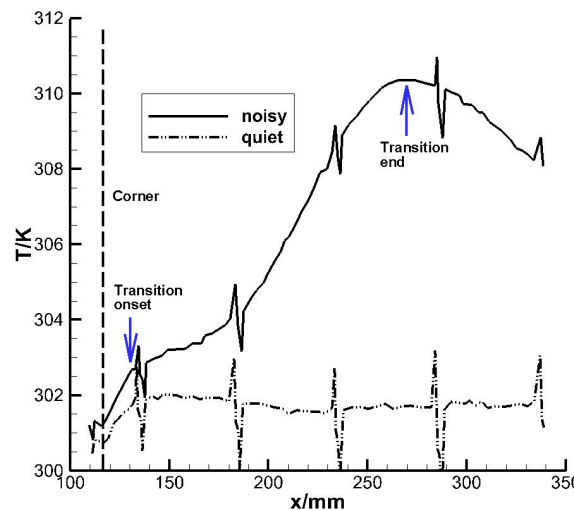


Figure 9: Centerline temperature for quiet and noisy flow condition for the X-51A inlet (from Ref [4])

## 4.2 Computational Results

Because the experimental model is symmetrical at the span-wise direction, the half model is used for computation to reduce the computational cost. In order to obtain the grid independent solution, three grids are used with refinement of the normal grid number from 61 to 241. The total grid number are 3.89, 5.31 and 8.43 million for three grids, respectively. The three grids are denoted by coarse grid, middle grid and refine grid. The  $y^+$  of the first layer of grid cells away from the wall is smaller than 1 for three grids.

Because the flow has not transition under the quiet mode, it is difficult to validate the grid-independent result for transitional computation so that only the transitional computation for the noisy mode is conducted to validate the grid-independent result.

As the turbulent intensity ( $Tu$ ) of free stream is unknown under quiet mode and noisy mode for Boeing/AFOSR Mach-6 Quiet tunnel, the  $Tu$  are 0.05% and 3% under quiet mode and noisy mode in

computation based on the noise level, respectively. For the transitional computation, the compressibility correction of Zheng<sup>[14]</sup> are used for transition model. Other choices will be also discussed in the next.

From Figure.10, the heat flux first decreases monotonically, then increase sharply at the corner, last increase gradually until to the turbulent heat flux. The transition onset has little change for three grids, but the transition finish position moves forward to the model tip from the coarse grid to the refine grid. The solution on the middle grid is very close to the grid independent solution. From the Figure.11, the turbulent solution has the same result as the transitional result. In conclusion, the middle grid is the most suitable one on account of the computational resolution and efficiency so that the below computation uses the middle grid.

Through the comparison among the laminar, transitional and turbulent heat transfer rate, the computational transition starts at  $x=130\text{mm}$  and finishes at  $x=260\text{mm}$ , whereas the experimental transition starts at  $x=134\text{mm}$  and finishes at  $x=270\text{mm}$ . The computational result agrees well with experiment. The transitional heat flux rate decreases before the corner. After the second oblique shock wave at the corner ( $x=116\text{mm}$ ), the heat flux rate increases monotonically until  $x=260\text{mm}$ . The turbulent heat flux has the same tendency as the transitional one except the sudden rise at the corner.

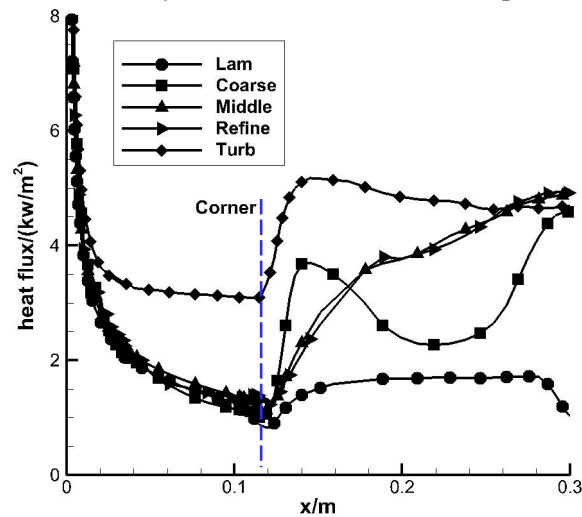


Figure 10: Transitional heat transfer rate along the wall centerline under noisy mode for the X-51A inlet on three grids

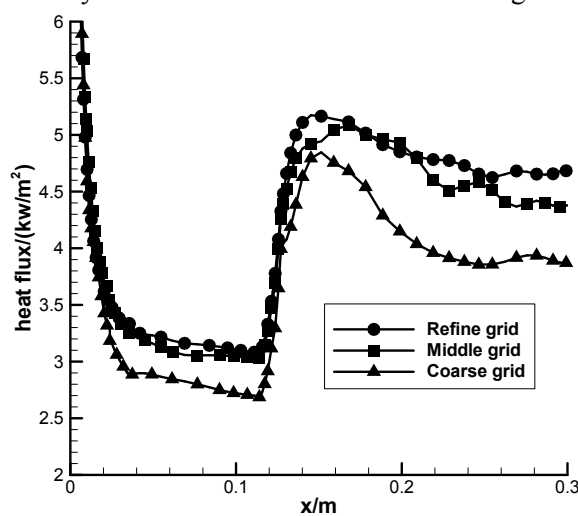


Figure 11: Turbulent heat transfer rate along the wall centerline under noisy mode for the X-51A inlet on three grids

From Figure.12, The first oblique shock wave is generated at the model tip, and the second oblique shock wave is generated from the corner between the forebody and the inlet. Both two

oblique shock waves are below the cowl by a small distance. The flow field under noisy mode is the same as that under quiet mode so that it is omitted for brevity. From Figure. 13, the inlet is in starting mode under quiet and noisy mode.

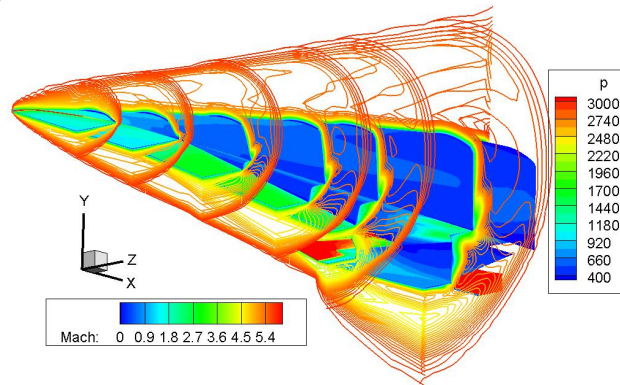


Figure 12: Mach number isolines at the cross-sections and pressure contour at the wall for X-51A inlet under quiet mode

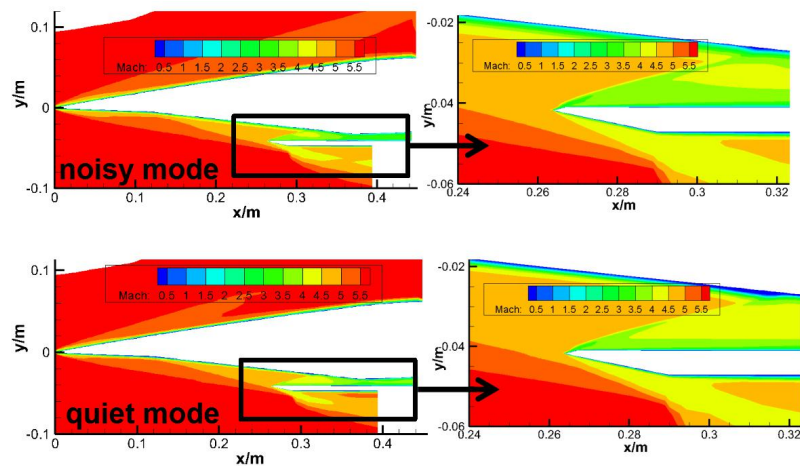


Figure 13: Mach number contour at symmetrical plane for X-51A inlet

From Figure.14, as like the experiment<sup>[4]</sup>, the flow remains laminar at the forebody under quiet mode, whereas the flow achieves the transition from laminar flow to turbulent flow at the forebody. From Figure.15, the transition region occurs earlier in the both span-wise end than that on the centerline from the experimental temperature measurement. However, the computed transition front makes little difference in the span-wise direction. It is shown that the transition prediction method needs further improvement. As like the SWL inlet, a small flow separation is generated at the isolator entrance on account of the interaction between reflected shock wave and the boundary layer (also shown in Figure. 14). No flow separation appears in the corner, which is different from the flow of SWL inlet.

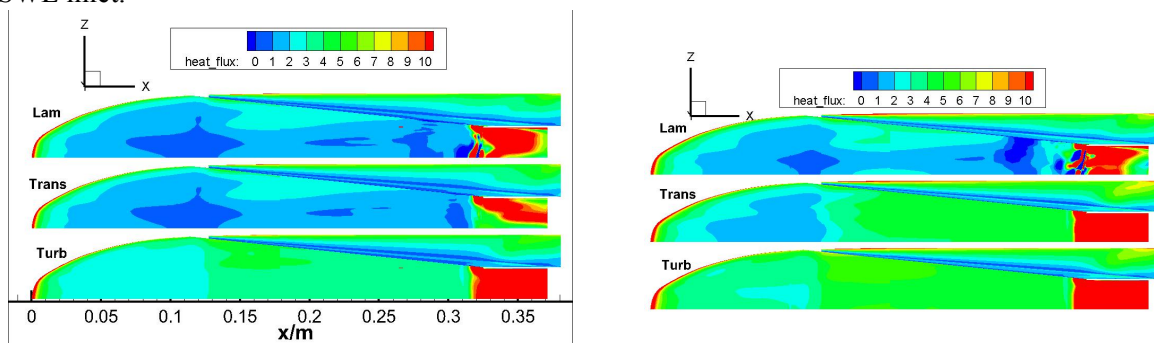


Figure. 14: heat flux contour of the wall of X-51A inlet under quiet mode (Left) and noisy mode (right)

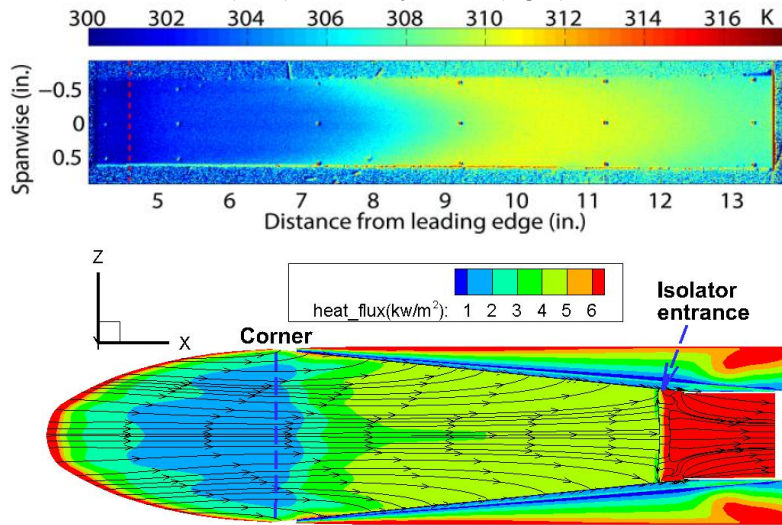


Figure. 15: Experimental surface temperature (top) and the computational heat flux and skin friction lines (bottom) of the wall of X-51A inlet under noisy mode

From Figure.16, the effect of compressibility corrections (i.e. equation (6)-(9) in section 2) on transitional region are compared with the heat flux rate. It should be noted that the flow transition starts at 134mm and finishes at 270mm away from the tip of model under noisy mode according to experiment. The langtry's result<sup>[3]</sup> gets too early transition onset before the corner and the finish position beside the corner. The Zhang's correction<sup>[13]</sup> get the same transition onset position after the corner as experiment, but later transition finish position than experiment. The Zheng's correction<sup>[14]</sup> is the best one in comparison with the experiment.

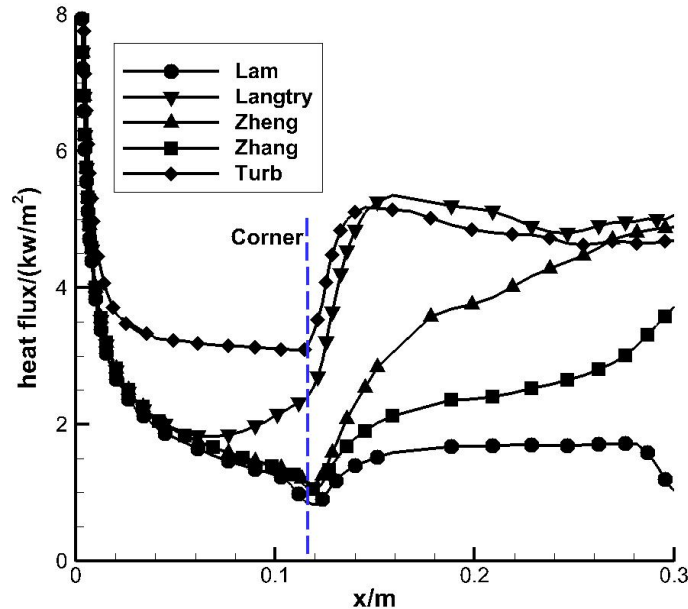


Figure 16: The effect of three correlation on transition region of the bottom wall plane of the X-51A inlet under noisy mode

It is difficult to directly compare the inlet performance between quiet mode and noisy mode because the unit Reynolds number of quiet mode is about 12% higher than that of noisy mode. In order to investigate the effect of turbulence intensity  $Tu$  on the inlet performance, two turbulence intensity are used for computation under quiet mode and noisy mode, respectively, to hold the same unit Reynolds number. One is low turbulence intensity of 0.05%, and the other is high turbulence

intensity of 3%. The results corresponding with the experiments are No.2 and No.3 in Table 2 for noisy mode and quiet mode, respectively.

From Table 2, after the comparison of No.2 and No.3, the noisy mode has higher mass flux than quiet mode because the total pressure  $P_t$  of noisy mode is 6% higher than that of quiet mode. The noisy mode has lower mass averaged Mach number  $Mw Ma$  and recovery coefficient of total pressure  $\sigma$  at the throat of inlet than quiet mode because the turbulent displacement thickness of boundary layer for noisy mode is larger than laminar displacement thickness for quiet mode, which generate stronger oblique shock waves for inlet. The  $Tu$  has minor effect on the mass flux rate but big effect on the recovery coefficient of total pressure and mass averaged Mach number. The smaller  $Tu$  has higher  $Mw Ma$  and  $\sigma$ .

Table 2 Effect of freestream disturbance on inlet performance

No.	Ma	$Re(*10^6/m)$	$Tu(\%)$	flux/(kg/s)	$Mw Ma$	$\sigma$
1	5.8	6.59	0.05	0.0455	3.157	0.580
2	5.8	6.59	3.00	0.0457	2.925	0.540
3	6.0	7.38	0.05	0.0385	3.211	0.602
4	6.0	7.38	3.00	0.0387	3.036	0.553

## 5 Conclusion and Future Work

Within this paper, the  $\gamma$ - $Re_{\theta t}$  transition model is improved with compressibility corrections of  $Re_{\theta t}$  and the cross-flow transition model. The transition model is used for transition prediction of two hypersonic inlets. One inlet is from the Shock Wave Laboratory (SWL) of RWTH Aachen University<sup>[2]</sup>, and the other inlet is the 20% scaled X-51A forebody in the Boeing/AFOSR Mach-6 Quiet tunnel<sup>[4]</sup>. The computational results shows a good agreement with experimental data. For two hypersonic inlet, the corner makes a great contribution to accelerate the transition.

For the 20% scaled X-51A forebody and inlet, the langtry's result<sup>[3]</sup> gets too early transition onset and finish position beside the corner. The Zhang's correction<sup>[13]</sup> get the same transition onset position after the corner as experiment, but later transition finish position than experiment. The Zheng's correction<sup>[14]</sup> is the best one in comparison with the experiment.

For the inlet performance, the laminar flow has the highest mass flux,  $Mw Ma$  and  $\sigma$ , and the turbulent flow has the smallest mass flux,  $Mw Ma$  and  $\sigma$ . The transitional flow is between the laminar and turbulent flow. The noisy mode has higher mass flux but lower mass averaged Mach number  $Mw Ma$  and recovery coefficient of total pressure  $\sigma$  than quiet mode. The  $Tu$  has minor effect on the mass flux rate but big effect on the recovery coefficient of total pressure and mass averaged Mach number. The small  $Tu$  has higher  $Mw Ma$  and  $\sigma$ .

Future work will focus on two aspects. One is the transition prediction of a hypersonic inlet at flight conditions. The other aspect is the forced-transition prediction as well as the trip design.

## References

- [1] S. A. Berry, K. Daryabeigi, and K. Wurster, Boundary layer transition on X-43A, *AIAA 2008-3736*, 2008.
- [2] Sarah Frauholz, Rirgit U. Reinartz, Siegfried, at. al., Transition prediction for scramjets using  $\gamma$ - $Re_{\theta t}$  model coupled to two turbulence models, *Journal of Propulsion and Power*, 2015,31(5):1404-1422.
- [3] R. B. Langtry, F. R. Menter, Correlation-based transition modeling for unstructured parallelized

- computational fluid dynamics codes, *AIAA J.* 2009, 47(12):2894-2906.
- [4] M. Borg, S. P. Schneider and T. J. Juliano, Effect of freestream noise on roughness-induced transition for the X-51A forebody, *AIAA 2008-0592*, 2008.
- [5] L. Xiao, L. Wang, Z. Xiao, et al., A modular RANS approach for modeling hypersonic flow transition on an air-breathing configuration, *AIAA-2013-0671*, 2013
- [6] Wang Liang and Fu Song., Development of an Intermittency Equation for the Modeling of the Supersonic/Hypersonic Boundary Layer Flow Transition, *Flow Turbulence Combust.* 2010, 87: 165-187.
- [7] M. Yi, H. Zhao and J. Le, Hypersonic natural and forced transition simulation by correlation-based intermittency model, *AIAA 2017-2337*, 2017.
- [8] Yoon S, Jameson A. Lower-upper symmetric Gauss-Seidel method for the Euler and Navier-Stokes equations. *AIAA Journal* 1988; 26(19):1025 - 1026.
- [9] K.H. Kim, C. Kim, O.H. Rho, Methods for the accurate computations of hypersonic flows, Part I: AUSMPW+ scheme, *Journal of Computational Physics*, 174 (2001) 38-8.
- [10] W.K. Anderson, J.L. Thomas, B. Van Leer, A comparison of finite volume flux vector splittings for the Euler equations, *AIAA 85-0122*, 1985
- [11] Menter, F.R., Two-Equation Eddy-Viscosity Turbulence Models for Engineering Applications, *AIAA Journal*, 32(8):1598-1605, 1994.
- [12] R. B. Langtry, K. Sengupta, D. T. Yeh, et. al., Extending the  $\gamma$ - $Re_{\theta t}$  local correlation based transition model for crossflow effects, *AIAA 2015-2474*, 2015.
- [13] Zhang Xiaodong, Gao Zhengong, A numerical research on a compressibility-correlated Langtry's transition model for double wedge boundary layer flows, *Chinese Journal of Aeronautics* 2011, 24:249-257.
- [14] Zheng Yun, Li Hong-yang, Application of  $\gamma$ - $Re_{\theta t}$  transition model in hypersonic flow based on new correlation equation, *Journal of Propulsion Technology* (in Chinese), 36(6):839-845, 2015.